

# Collisional S-Matrix for the Vibrational Dynamics of H+H<sub>2</sub> Including Dissociative Processes by Quantum Computing

*Yulun Wang and Predrag S. Krstic*

Institute for Advanced Computational Science, Stony Brook University,  
Stony Brook NY 11794-5250

## ABSTRACT

Quantum circuit is developed and applied to compute accurately S matrix for the transitions between vibrational states of H<sub>2</sub> in collisions with H at 100 eV laboratory collision energy. The effects of the discretized dissociative continuum to the transition cross sections are carefully studied and the maximum number of continua is found to provide convergence of the results within 5%. The results were confirmed by comparison with independent ODE solution of the time-dependent Schrodinger equation and comparison with few results form literature.

## 1. INTRODUCTION

Hydrogen atom colliding with hydrogen molecule is the most fundamental neutral atom-molecule collision systems. Detailed knowledge of the inelastic and elastic processes is of high importance in the star formation processes from molecular clouds, but also in energy and particle redistribution of fusion divertor plasma, especially when hydrogen molecules are vibrationally excited. Vibrationally excited molecules have significantly enhanced dissociation. Vibrationally excited states of H<sub>2</sub> are formed by associative desorption, collisional neutralization, and excitation on the plasma-facing material surfaces, and possibly, by three-body diatomic association in  $H + H + H$  collision. In addition, the elastic scattering at excited vibrational states of abundant hydrogen molecules can play important role in transport and dissipation of the divertor plasma momentum [1-6].

A typical collision event evolves through dynamically coupled electronic, vibrational and rotational degrees of freedom. Historically, these systems have been studied thoroughly only for the processes from the ground states (electronic, vibrational, rotational) as motivated by applications, as well as limited by experimental and theoretical capabilities of the time [3]. Also, the corresponding calculations were usually done within a manifold of bound vibrational states, thus neglecting the possible importance of inelastic processes through dissociative channels, as well as the dynamic change of the dissociative continuum edge with the position of the projectile [5,6].

Paul Benioff and Richard Feynman [7,8] have proposed the idea of quantum computing in 1980s, predicting advantages of quantum algorithms in a quantum computer for simulating complex

quantum mechanical system. Classical computing faces difficulties in, for example, eigenvalue problems of many-body quantum systems, and transition dynamic among excited states. Despite all the challenges and difficulties to build a satisfying fault-free quantum computer in the near future, an increasing amount of effort is invested to develop quantum algorithms with this new perspective. In this work we aimed to develop an algorithm for a quantum computer that would be able to calculate the collisional S-matrix [5,6,9] for transitions between dissociating vibrational states at the ground electronic surface of  $H_2$  ( $X^1\Sigma_g^+$ ) in collision with  $H$  (1s). A peculiarity of the present calculation is inclusion of the dissociative continuum in the calculation. The finite set of the bound vibrational states can be considered as a closed quantum system in presence of the interactions with the dissociative “environment”, in which case the calculated  $S$  matrix will be for an open quantum system. Thus, current calculation is a possible test ground (not pursued here) for quantum computing methods for the open systems approximations in the Lindblad type of equations.

For the  $H_3$  ground surface we adopt the analytical fit of Boothroyd [10], augmented with HF-CI results of Krstic et al [9] at distances between any two atoms smaller than 1 *a.u.* We build the algorithm and system of quantum circuits to calculate evolution operator of the system in Trotter approximation, from which we obtain the  $S$ -matrix and relevant cross sections. As basis for the expansion of exponential operators we use eigenstates of the unperturbed vibrational Hamiltonian  $H_0$  of  $H_2$  (atomic system of units,  $\hbar = m_e = e = 1$ , is used throughout the paper unless specified differently)

$$H_0\varphi = \left( -\frac{1}{2\mu} \frac{\partial^2}{\partial r^2} + V_{H_2}(r) \right) \varphi(r, t) = \varepsilon\varphi \quad (1)$$

where  $r$  is the vibrational coordinate and  $\mu$  is the reduced mass of  $H_2$  ( $\sim 0.5$  *a.m.u.*). This eigenvalue problem was solved with finite quantization “volume” boundary conditions,  $\varphi_k^{(n)}(r_{\max}) = \varphi_k^{(n)}(r_{\min}) = 0$ , where  $r_{\max} = 20$  and  $r_{\min} = 0.02$ , with  $n = 256$  mesh point along the  $r$ -axis. This resulted in 256 vibrational states on each of  $H_2$ , with 15 bound and 241 continuum (positive energy) pseudo-states. Although the relevant vibronic continua are discretized, with this choice of  $r_{\max}$  the density of continuum states (largest close to the continuum edge) stays high enough even for several eV above the continuum edge. The discretization of the dissociative continuum was used earlier by Krstic et al [6] to calculate dissociation in the  $H_3^+$  collision system at collision energies below 10 eV.

The excitation energy of the first vibrational state of  $H_2$  is  $\sim 0.5$  eV corresponding to a characteristic vibration time exceeding 50 a.u., which is comparable to the collision time of the order of  $\left(\frac{\mu}{2E}\right)^{1/2}$  for energies  $< 100$  eV. The collision time is still short compared to the time scale of molecular rotations (excitation energy 0.01 eV, i.e., the characteristic times  $> 1000$  a.u.), thus enabling one to consider the direction of the diatomic internuclear axis as fixed. The consequence is that the angle  $\gamma$ , defined as the angle between  $\vec{R}$  (defined from the center of mass of the molecule to the

projectile nucleus) and diatomic internuclear axis  $\vec{r}$ , stays constant during a collision, i.e., enters the theory as a parameter. In effect, the equations of motion are completely decoupled as far as the angular variables are concerned. We are adopting in this work  $\gamma = 90^\circ$ , and present the geometry of the collision in the Jacobi coordinates  $(\vec{R}, \vec{r}, \gamma)$ .

Fully quantal approach discussed above, is not practical at higher energies (few tens eV) because of too large number of partial waves involved. An alternative is to replace the partial wave with the impact parameter formalism, assuming a classical motion of the projectile. Vibrational motion should be still treated quantally, on the lowest adiabatic electronic surfaces of the  $H_3$ , while diatomic target rotations are frozen. The resulting time-dependent Schrodinger equation for the nuclear motion, within Born-Oppenheimer approximation, is

$$H\Psi(R(t), r, t) = (H_0 + V(R(t), r))\Psi(R(t), r, t) = i \frac{\partial \Psi(R(t), r, t)}{\partial t} \quad (2)$$

where  $R(t)$ , is the projectile displacement with respect to diatomic center-of mass defined here in the straight line approximation,  $R = \sqrt{b^2 + v^2 t^2}$ , where  $b$  is the impact parameter, and  $v$  is the velocity of the projectile with respect to the center of mass of  $H_2$ , calculated as  $v = \sqrt{\frac{2E_{CM}}{M}}$ , where  $E_{CM}$  is center of mass energy, taken here to be  $\frac{100}{3}$  eV, and  $M$  is the reduced mass of the  $H + H_2$  molecule,  $M \sim \frac{1}{3}$  a. m. u.

The assumption of the classical motion of hydrogen atom at this velocity is acceptable, since its corresponding De Broglie wavelength of the hydrogen is about 0.05 Bohrs, much smaller than the characteristic dimension of the  $H_2$  molecule and characteristic interaction radius of  $H$  and  $H_2$ . Finally,

$$V(R, r) = V_{H_3}(R, r) - V_{H_2}(r) \quad (3)$$

where  $V_{H_3}(R, r)$  is the ground potential adiabatic surface of  $H_3$  molecule. A nice feature of such defined  $V(R, r)$  is that  $V(R \rightarrow \infty, r) = 0$  which enables correct definition of the initial and final states in the  $S$  matrix.

In Section 2 we develop our method and quantum circuits for calculation of the  $S$  matrix for the vibrational dynamics of  $H_2$  in collision with  $H$ , including the dissociative continuum. In Section 3 we show our results for the cross sections of transitions with bound vibrational states, as well as for the dissociation. We verify our results obtained from simulation using quantum circuits by comparison with benchmark, which we obtain by solving time dependent Schrodinger equations as system of ordinary differential equations (ODE), using the expansion of the  $H + H_2$  wavefunction in vibrational basis of  $N = 256$  states,

$$\Psi(\vec{r}, t) = \sum_{i=1}^N c_i |\varphi_i\rangle \quad (4)$$

Finally, our conclusions are presented in Section 4.

## 2. METHOD

Eq. 2 is solved on a numerical mesh, employing the split-operator technique in the energy representation. Iterating the state vector in time from some large initial “ $-T$ ”:

$$\Psi(t) = e^{-i \int_{-T}^t H(t') dt'} \quad (5a)$$

which can be iterated with a small step  $\tau$  starting from  $\Psi_0 = \Psi(-T)$  and following the ordering of time:

$$\begin{aligned} \Psi_1 &= e^{-i\tau H(t_1)} \Psi_0 \\ \Psi_2 &= e^{-i\tau H(t_2)} \Psi_1 \\ &\dots \\ \Psi_n &= e^{-i\tau H(t_n)} \Psi_{n-1} \end{aligned} \quad (5b)$$

where  $t_n = -T + n\tau$  and  $\tau = \Delta t$ . Since  $H$  is moving classically,  $R = R(t)$ , and  $R_{max}$  is chosen large enough so that  $H$  is not interacting at  $t = -T$  with  $H_2$ . Then  $\Psi(-T) = \Psi_0$  is an unperturbed initial vibrational state, which could be any bound  $\varphi_i(r)$  or a linear combination of  $\varphi_i(r)$ 's. In this paper we do not consider a dissociative state of  $H_2$  as an initial state.  $\Delta t$  is chosen small enough to have desired transition probabilities  $|\langle \varphi_i | \Psi(T) \rangle|^2$  emerging from initial  $\Psi(-T)$  deviate from the benchmark ODE solution less than a given error.

### 2.1. Preparing qubit Hamiltonian

With the discrete  $N$ -state vibrational basis  $\{|\varphi_i\rangle\}$ , defined in Eq. 1, one can write the Hamiltonian operator as:

$$H = \sum_{i,j=0}^{N-1} h_{ij} |\varphi_i\rangle \langle \varphi_j| \quad (6)$$

where the matrix elements of  $H$  in Eq. 6 in the chosen basis set are defined as:

$$h_{ij}(R(t)) = \langle \varphi_i | H | \varphi_j \rangle \quad (7)$$

One can go to the second quantization of the Hamiltonian, which would replace the excitation operator  $|\varphi_i\rangle \langle \varphi_j|$  from state  $j$  to state  $i$  with the corresponding operator of creation and annihilation of population of the vibrational states, i.e., with  $a_i^\dagger a_j$ .

In this work, we utilize the Qubit Efficient Encoding (QEE) [11] method to map the vibrational Hamiltonian to qubit Hamiltonian. With the QEE mapping, a  $N$ -state system can be encoded using  $n = \log_2 N$  qubits, making full use of all qubit computational basis. With the chosen vibrational basis set  $\{|\vec{\varphi}\rangle\}$ , the  $i^{th}$  state of the system  $|\varphi_i\rangle$  is encoded to the  $i^{th}$  qubit computational basis of  $n$  qubits  $|\mathbf{q}_i\rangle$ , which can be expressed in individual qubits  $|\mathbf{q}_i\rangle = |y_{n-1}, \dots, y_0\rangle$  with  $y \in \{0,1\}$ . Thus, 256 vibrational states are encoded with a complete computational basis of  $n = 8$  qubits. Hence one can write the qubit Hamiltonian as:

$$H_q(R) = \sum_{i,j=0}^{N-1} h_{ij} |\mathbf{q}_i\rangle\langle\mathbf{q}_j| \quad (8)$$

$|\mathbf{q}_i\rangle\langle\mathbf{q}_j|$  is now the qubit excitation operator which enables the transition from state  $|\mathbf{q}_j\rangle$  to state  $|\mathbf{q}_i\rangle$ :  $(|\mathbf{q}_i\rangle\langle\mathbf{q}_j|)|\mathbf{q}_j\rangle = |\mathbf{q}_i\rangle$ . It can be further factorized to individual qubits with the expression:  $\otimes \prod_{k=0}^{n-1} |y_k^i\rangle\langle y_k^j|$ , where  $k$  is the index of qubits, which can be replaced by Pauli operations to obtain a full qubit Hamiltonian:

$$\begin{aligned} |0\rangle\langle 0| &= \frac{1}{2}(I + Z), |1\rangle\langle 1| = \frac{1}{2}(I - Z) \\ |0\rangle\langle 1| &= \frac{1}{2}(X + iY), |1\rangle\langle 0| = \frac{1}{2}(X - iY) \end{aligned} \quad (9)$$

After simplification, the qubit Hamiltonian can be written as a linear combination of complex coefficients with Pauli quantum operations:

$$H_q = \sum_k g_k P_k \quad (10)$$

where  $g_k$  is the linear combination of  $h_{pq}$  and  $h_{pqrs}$  coefficients and  $P_k \in \{I, X, Y, Z\}^{\otimes n}$  represent the  $n$ -fold tensor product of Pauli operators. The number of terms in qubit Hamiltonian  $m$  follows an exponential correlation with the number of qubits  $n$  used to encode the system:  $m = 4^n$ , which is the number of total combinations of  $n$ -fold Pauli operators.

For example, the qubit Hamiltonian of a general 4-state system using 2 qubit takes the form:

$$\begin{aligned} H_q &= g_0 I + g_1 Z_0 + g_2 Z_1 + g_3 Z_0 Z_1 + g_4 X_0 + g_5 X_1 + g_6 Y_0 + g_7 Y_1 + g_8 X_0 Z_1 \\ &+ g_9 Y_0 Z_1 + g_{10} Z_0 X_1 + g_{11} Z_0 Y_1 + g_{12} X_0 X_1 + g_{13} Y_0 Y_1 + g_{14} X_0 Y_1 + g_{15} Y_0 X_1 \end{aligned} \quad (11)$$

where coefficients  $g_i$ ,  $i = 0, \dots, 15$  are time-dependent real numbers, built of  $h_{ij}(t)$ , and derived in Sec. S1 of SM.

## 2.2. Calculation of the matrix elements of Hamiltonian

The basic building elements of our algorithm are matrix elements of the total Hamiltonian  $H$ , defined in Eq. 2, using extended vibrational basis, defined by Eq. 1

$$h_{ij}(R(t)) = \langle\varphi_i|H|\varphi_j\rangle = \left\langle\varphi_i\left|H_0 + \left(V_{X^1\Sigma_g^+}(R, r) - V_{H_2}(r)\right)\right|\varphi_j\right\rangle = \varepsilon_i \delta_{ij} + V_{ij}(R) \quad (12)$$

where  $\varepsilon_i$  ( $i = 0, \dots, N - 1$ ) are eigenstates of the vibrational Hamiltonian  $H_0$  obtained as described following Eq. 1. The lowest 15  $\varepsilon_i$ 's are negative, presenting the bound vibrational states, the other 241 are states of the vibrational continuum, having positive energy. The energy spectrum of  $\{\varepsilon_i\}$  is shown in Fig. 1 for the first 150 vibrational states.

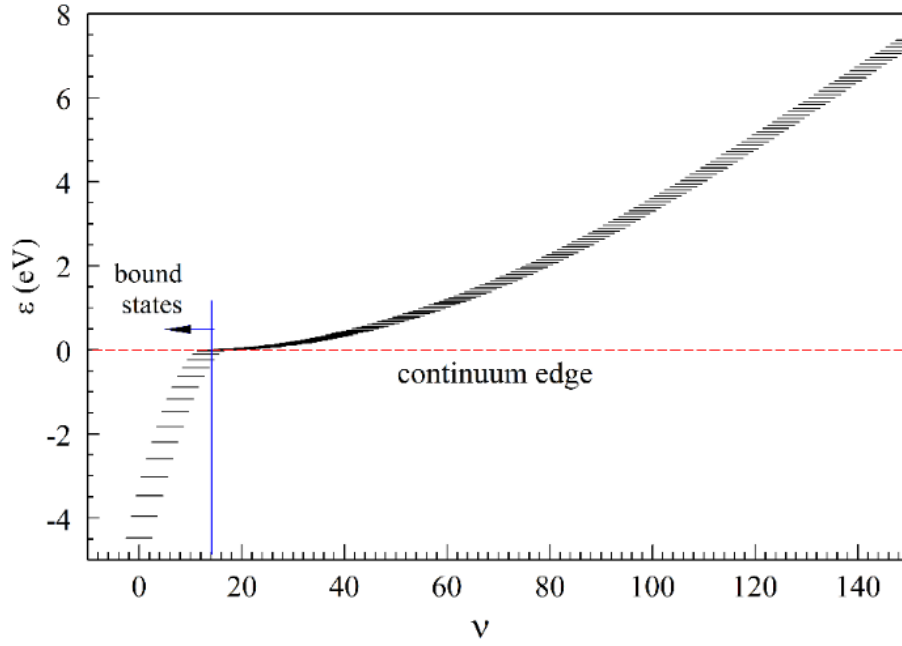


Fig. 1. Discretized energy spectrum of the first 150 vibrational states of  $H_2$ .

$V_{ij}(R)$  are calculated by numerical integration for all combinations  $ij$ , where  $i = 0, \dots, 255, j = i, \dots, 255$ , in steps  $\Delta R = 0.1$ , from  $R = 0$  to  $R = 20$ . Symmetry  $h_{ij}(R) = h_{ji}(R)$  is used in further calculation. Several typical matrix elements (ME)  $h_{ij}(R)$  are shown in Fig.2. Their values in all cases decrease fast to the negligible values when  $R$  increases.

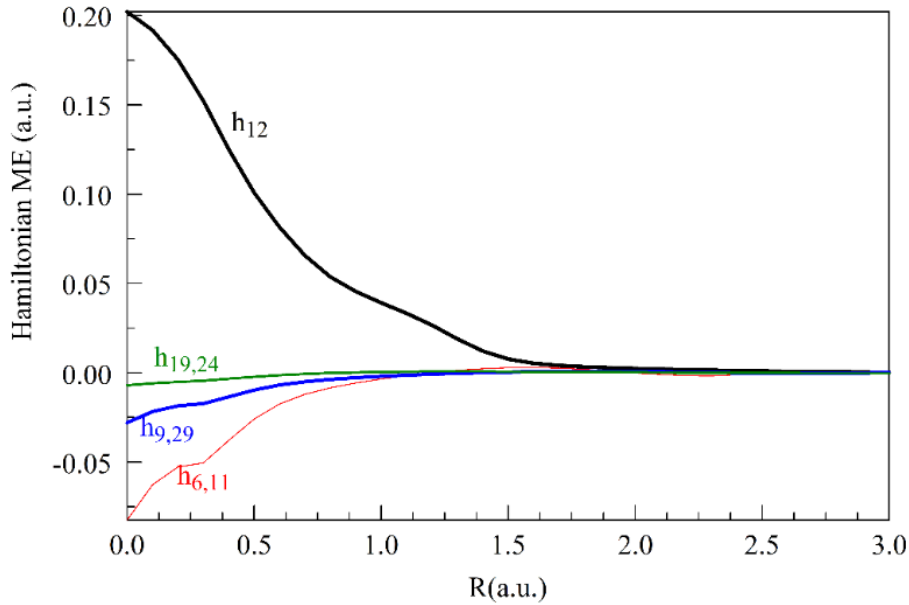


Fig. 2. Typical matrix elements  $h_{ij}(R)$  of  $H$  in vibrational basis.

For iteration of the system wave function by split-operator technique, the size of the time step

$\tau$  was evaluated in order to find the optimal one by verifying with the benchmark ODE solution of the time-dependent Schrodinger equation. The ODE solution has reached relative accuracy of  $10^{-6}$  with time step  $\tau = 0.001$ . It was found that  $\tau = 0.1$  has produced by split operator technique relative deviation from the benchmark solution less than 1%.

In order to obtain  $h_{ij}(R(t))$  at all needed instances of time, the obtained  $h_{ij}(R)$  was fitted for the desired times using fourth order splines. We note that the evolution time of the system was varied from  $t = -T$  to  $t = T$ , where  $T = T(b) = \sqrt{R_{\max}^2 - b^2}/v_H$  and  $R_{\max} = 20$ . Thus, for  $b = 0.01$ , we find that  $V_{ij}(R_{\max}) < 10^{-6}$ . The fitting to the desired time instances was done for each impact parameter, used in calculation of the cross sections. We have done calculation for one angle  $\gamma = \gamma(\vec{R}, \vec{r}) = 90^\circ$ .

### 2.3. Trotterization of evolution operator

To simulate the time dependent evolution on a quantum computer, the evolution operator at time  $t$ ,  $U(t, t - \tau) = e^{-i\tau H_q(R(t))}$ , needs to be applied for each timestep  $\tau$ , strictly following the time ordering. For simplicity,  $U(t, t - \tau)$  will be written as  $U(t)$  from now on. Then following Eq. 5b, one can combine  $U(t)$  at each discrete timestep together, the overall time evolution operator  $U$  can be obtained:

$$U = U(T) \cdots U(-T + 2\tau)U(-T + \tau) = \prod_{t_d=-T}^{-T+\tau} e^{-iH_q(R(t_d))\tau} \quad (13)$$

where  $-T$  is the initial time,  $T$  is final time and  $t_d$  is the discrete time points.

We note that  $H_q(R_1)$  and  $H_q(R_2)$  do not commute if  $R_1 \neq R_2$ . However, in order to calculate  $U(t)$  one needs to factor it into individual Pauli operators. In general, the Pauli terms  $P_k$  in the qubit Hamiltonian do not commute with each other. Hence the evolution operator  $e^{-i\tau H_q(R(t))} = e^{-i\tau \sum_{k=1}^m g_k(R(t))P_k}$  cannot be exactly factored as  $\prod_{k=1}^m e^{-i\tau g_k(R(t))P_k}$ . A proper approximation of evolution operator can be utilized here for an accurate simulation, such as Trotterization. For qubit Hamiltonian with  $m$  terms, the second order Suzuki-Trotter gives:

$$e^{-i\tau \sum_{k=1}^m g_k P_k} = \left( e^{-\frac{i\tau g_1 P_1}{2}} e^{-\frac{i\tau g_2 P_2}{2}} \cdots e^{-\frac{i\tau g_{m-1} P_{m-1}}{2}} e^{-i\tau g_m P_m} e^{-\frac{i\tau g_{m-1} P_{m-1}}{2}} \cdots e^{-\frac{i\tau g_2 P_2}{2}} e^{-\frac{i\tau g_1 P_1}{2}} \right) + O(m^3 \tau^3) \quad (14)$$

Each term in Eq. 14,  $e^{-\frac{i\tau g_k P_k}{2}}$ , can be applied by quantum circuits, discussed in detail in Subsection 2.4. Applying Trotterization of a higher order can improve the accuracy, but at the cost of more terms leading to much longer computational time [12]. The choice of Trotterization method should be made with careful tradeoff.

## 2.4. Quantum circuit for simulating time evolution

The operator  $e^{-\frac{i\tau g_k P_k}{2}}$  in Eq. 14 with  $P_k \in \{I, X, Y, Z\}^{\otimes n}$  as the  $n$ -fold tensor product of Pauli operators can be applied using the quantum circuits. However, the exponentiation of  $n$ -fold  $P_k$  is a complex quantum operation which requires a further decomposition to the elementary qubit operations such as *CNOT* gate and the single qubit gates that can be executed directly by quantum computers. The decomposition is done in two steps.

In the first step,  $e^{-\frac{i\tau g_k P_k}{2}}$  is decomposed to the  $n$ -fold tensor product of Pauli- $Z$  and  $I$  matrices  $e^{-\frac{i\tau g_k A}{2}}$  ( $A \in \{I, Z\}^{\otimes n}$ ) and a few single qubit gates [13]. For simplicity, one can express  $P_k$  and  $A$  in individual qubits:  $P_k = \bigotimes \prod_{i=1}^n p_{k,i}$  and  $A = \bigotimes \prod_{i=1}^n \alpha_i$ , where  $p_{k,i} \in \{I, X, Y, Z\}$  and  $\alpha_i \in \{I, Z\}$  are the single qubit gates of  $i^{th}$  qubit. If  $p_{k,i} = X$ ,  $\alpha_i = Z$  and one Hadamard gate will be added on  $i^{th}$  qubit on each side of  $e^{-\frac{i\tau g_k A}{2}}$  operation. If  $p_{k,i} = Y$ ,  $\alpha_i = Z$  and  $R_X\left(\frac{\pi}{2}\right)$  and  $R_X\left(-\frac{\pi}{2}\right)$  gates will be added on  $i^{th}$  qubit on the left and right side of  $e^{-\frac{i\tau g_k A}{2}}$  operation respectively, where  $R_X(\theta)$  is the single qubit rotation gate around  $x$ -axis with an angle of  $\theta$  defined as:

$$R_X(\theta) = e^{-i\frac{\theta}{2}X} = I \cos \frac{\theta}{2} - iX \sin \frac{\theta}{2} = \begin{bmatrix} \cos \frac{\theta}{2} & -i \sin \frac{\theta}{2} \\ -i \sin \frac{\theta}{2} & \cos \frac{\theta}{2} \end{bmatrix} \quad (15)$$

If  $p_{k,i} = Z$  or  $I$ ,  $\alpha_i = Z$  or  $I$  and no single qubit operation will be added on  $i^{th}$  qubit.

For example, in a 4-qubit case  $e^{-\frac{i\tau g_k}{2}(X \otimes I \otimes Y \otimes X)}$  operation can be decomposed to a circuit of  $e^{-\frac{i\tau g_k}{2}(Z \otimes I \otimes Z \otimes Z)}$  operation and several single qubit gates, shown in Fig. 3.

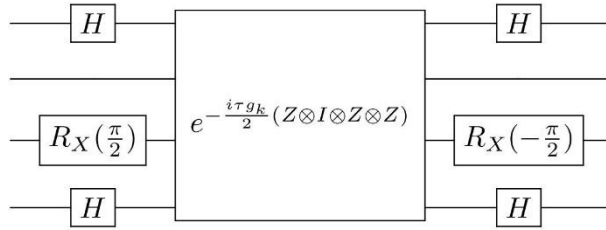


Fig. 3. An example of decomposing  $e^{-\frac{i\tau g_k}{2}(X \otimes I \otimes Y \otimes X)}$  to a circuit of  $e^{-\frac{i\tau g_k}{2}(Z \otimes I \otimes Z \otimes Z)}$  operation and several single qubit gates.

In the second step, the operator  $e^{-\frac{i\tau g_k A}{2}}$  will be further decomposed to *CNOT* gates and  $R_Z(\tau g_k)$  rotation gates [13], where  $R_Z(\theta)$  is the single qubit rotation gate around  $z$ -axis with an angle

of  $\theta$  defined as:

$$R_Z(\theta) = e^{-i\frac{\theta}{2}Z} = I \cos \frac{\theta}{2} - iZ \sin \frac{\theta}{2} = \begin{bmatrix} e^{-i\frac{\theta}{2}} & 0 \\ 0 & e^{i\frac{\theta}{2}} \end{bmatrix} \quad (16)$$

This can be easily achieved by applying one  $R_Z(\tau g_k)$  and connecting neighboring  $i^{th}$  and  $j^{th}$  qubits by  $CNOT$  gate at both sides of  $R_Z(\tau g_k)$  if  $\alpha_i = \alpha_j = Z$ . If  $\alpha_i = I$ , it will be omitted by  $CNOT$  gates. An example of the circuit for decomposing  $e^{-\frac{i\tau g_k}{2}(Z \otimes I \otimes Z \otimes Z)}$  is shown in Fig. 4.

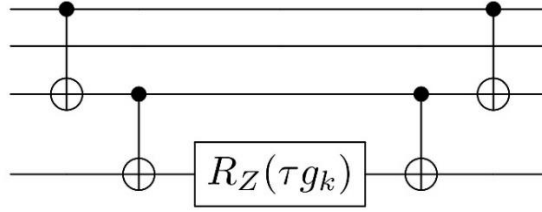


Fig. 4. An example of decomposing  $e^{-\frac{i\tau g_k}{2}(Z \otimes I \otimes Z \otimes Z)}$  to a circuit of  $R_Z$  gate and  $CNOT$  gates.

After two steps of decomposition, the operator  $e^{-\frac{i\tau g_k P_k}{2}}$  is a quantum circuit ready to be applied on a quantum computer. Then the evolution operator  $U(t) = e^{-i\tau H_q(R(t))}$  at time  $t$ , which is a product of many  $e^{-\frac{i\tau g_k(R(t))P_k}{2}}$  terms after Trotterization, can be expressed by the quantum circuit. Furthermore, by grouping all evolution operators for each time step as a product following Eq. 13, the quantum circuit of overall evolution operator  $U(T)$  is obtained and shown in Fig. 5.

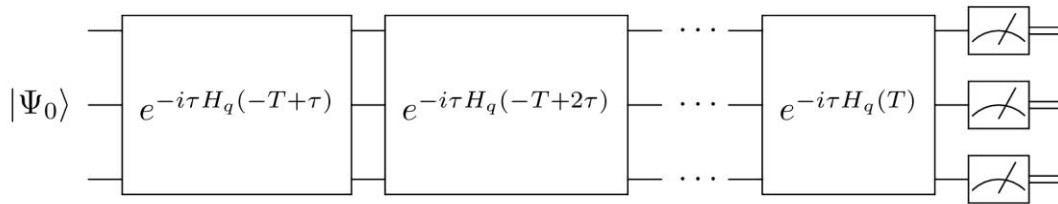


Fig. 5. The quantum circuit for simulating time evolution. The circuit is initialized in state  $\Psi_0$ . Each box represents the evolution operator for a time step of size  $\tau$ . The circuit ends with the measurements of the final transition probabilities.

Note that evolution operator  $U(t)$  at each time step shares the same structure of quantum circuits, but different time-dependent coefficients  $g_k(R(t))$  are loaded in the circuit at each time step. With an initial state  $\Psi_0 = \Psi(-T)$  defined, the circuit will have the final state  $\Psi(T) = U\Psi(-T)$  at the end of evolution. The final transition probabilities can be obtained upon measurements of multiple shots.

## 2.5. Calculation of the S-matrix

The  $S$ -matrix is a unitary matrix that relates the initial and final states of a physical system which undergoes a scattering process. It is important to stress that initial and final states of the system related by the  $S$ -matrix are defined in absence of the interaction which causes the transitions. Each column of the  $S$ -matrix contains transition amplitudes from one initial state to all possible final states. If the initial state of the system is a mixture of populations of various eigenstates of the system, the final state will be described by the coherent combination of various  $S$ -matrix elements, implying the interference of the complex transition amplitudes. In this work, the  $S$  matrix element for transition from the state  $|i\rangle$  to the state  $|j\rangle$  is:

$$S_{ji} = \langle j|U|i\rangle = \langle j|\prod_{k=1}^M e^{-i\tau H_q(R(t_k))}|i\rangle \quad (17)$$

where  $t_k = -T + k\tau$ ,  $M$  is the number of time steps and  $U$  is the unitary operator representing the overall time evolution.

Hence the  $S$ -matrix operator is expressed as:

$$S = \prod_{k=1}^M e^{-i\tau H_q(R(t_k))} \quad (18)$$

which in quantum circuit representation is equivalent to the overall time evolution operator  $U$  introduced in Subsection 2.4. Following qubit efficient encoding, the  $S$ -matrix operator can be written as:

$$S = \sum_{i,j=0}^{N-1} S_{ij} |\mathbf{q}_i\rangle \langle \mathbf{q}_j| \quad (19)$$

where  $|\mathbf{q}_i\rangle$  and  $|\mathbf{q}_j\rangle$  are encoded qubit computational basis state and each element of the  $S$ -matrix is:

$$S_{ij} = \langle \mathbf{q}_i|U|\mathbf{q}_j\rangle. \quad (20)$$

In this section, we propose a quantum module to calculate the full  $S$ -matrix using a quantum computer. The quantum circuit to calculate the real part of expectation value  $\langle \mathbf{q}_i|U|\mathbf{q}_j\rangle$  is shown in Fig. 6. It requires two quantum registers: one register with  $n$  qubits (e.g., for 256-state system,  $n = 8$ ) enough to load the quantum states  $|\mathbf{q}_i\rangle$  and  $|\mathbf{q}_j\rangle$ , and another register with an ancilla qubit. At the end, only ancilla qubit is measured to give the value of  $Re[\langle \mathbf{q}_i|U|\mathbf{q}_j\rangle]$ .

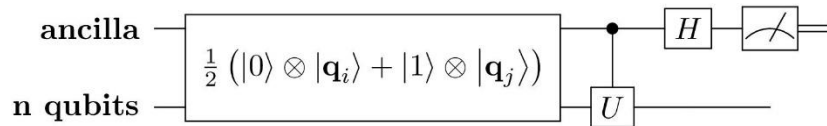


Fig. 6. The quantum circuit to calculate the  $Re[\langle \mathbf{q}_i|U|\mathbf{q}_j\rangle]$ . The quantum registers are initialized in the state  $\frac{1}{\sqrt{2}}(|0\rangle + |1\rangle) \otimes |\mathbf{q}_i\rangle$ .

At the first step, the quantum circuit is initialized in the state:

$$\frac{1}{\sqrt{2}}(|0\rangle \otimes |\mathbf{q}_i\rangle + |1\rangle \otimes |\mathbf{q}_j\rangle) \quad (21)$$

The controlled- $U$  operation is applied from ancilla to the rest of qubits, resulting in the state:

$$\frac{1}{\sqrt{2}}(|0\rangle \otimes |\mathbf{q}_i\rangle + |1\rangle \otimes U|\mathbf{q}_j\rangle) \quad (22)$$

Note that  $U$  is the overall evolution operator.

After a Hadamard gate on the ancilla qubit in Fig. 6 the quantum state becomes:

$$\begin{aligned} & \frac{1}{\sqrt{2}}(|+\rangle \otimes |\mathbf{q}_i\rangle + |-\rangle \otimes U|\mathbf{q}_j\rangle) \\ &= \frac{1}{\sqrt{2}}(|0\rangle \otimes (|\mathbf{q}_i\rangle + U|\mathbf{q}_j\rangle) + |1\rangle \otimes (|\mathbf{q}_i\rangle - U|\mathbf{q}_j\rangle)) \end{aligned} \quad (23)$$

The probability of measuring ancilla qubit in state  $|0\rangle$  is:

$$p_0 = \frac{1}{4}(2 + \langle \mathbf{q}_i | U | \mathbf{q}_j \rangle + \langle \mathbf{q}_j | U^\dagger | \mathbf{q}_i \rangle) = \frac{1}{2}(1 + \text{Re}[\langle \mathbf{q}_i | U | \mathbf{q}_j \rangle]) \quad (24)$$

Hence the value of  $\text{Re}[\langle \mathbf{q}_i | U | \mathbf{q}_j \rangle]$  is equal to the difference of probabilities measuring ancilla qubit in state  $|0\rangle$  and  $|1\rangle$ :

$$\text{Re}[\langle \mathbf{q}_i | U | \mathbf{q}_j \rangle] = 2p_0 - 1 = p_0 - p_1 \quad (25)$$

Similarly, to obtain the imaginary part of expectation value  $\langle \mathbf{q}_i | U | \mathbf{q}_j \rangle$ :  $\text{Im}[\langle \mathbf{q}_i | U | \mathbf{q}_j \rangle]$ , the circuit needs to be initialized in state:

$$\frac{1}{\sqrt{2}}(|0\rangle \otimes |\mathbf{q}_i\rangle - i|1\rangle \otimes |\mathbf{q}_j\rangle) \quad (26)$$

Following the same steps as shown in Eqs. 22-25, the value of  $\text{Im}[\langle \mathbf{q}_i | U | \mathbf{q}_j \rangle]$  is obtained as:

$$\text{Im}[\langle \mathbf{q}_i | U | \mathbf{q}_j \rangle] = 2p_0 - 1 = p_0 - p_1 \quad (27)$$

## 2.6. Computation of the ODE benchmark

By expanding the wavefunction in a set of vibrational basis states (as shown in Eq. 4), the time-dependent Schrodinger equation is approximated by a system of ODEs, which is solved by high accuracy classical methods and used as the benchmark to the results obtained by the quantum computing simulations. The set of coupled ODEs is solved using the explicit Runge-Kutta method of orders 5 and 4 (RK45, using Python `scipy.integrate.solve_ivp` function [14]). The accuracy is set by absolute and relative tolerance at each step of  $10^{-12}$  and  $10^{-6}$  respectively. The obtained transition amplitudes and probabilities with a time step size  $\tau = 0.01$  a.u. are used to provide cross-sections in Sec.3. The deviations of quantum algorithm results are compared with ODE benchmark results in the last part of Sec.3.

### 3. RESULTS

We calculated the transition probabilities  $P_{ij}$  for specific cases of initial and final states,  $|i\rangle$  and  $|j\rangle$ , for various values of impact parameter  $b$ . The cross section can then be obtained as:

$$\sigma_{i-j} = 2\pi \int b P_{ij}(b) db \quad (28)$$

We also calculate the cross sections for dissociation of a bound vibrational state  $|i\rangle$  by summation of the probabilities for transition for  $|i\rangle$  to all included states of dissociative continuum  $|j_D\rangle$ :

$$\sigma_{i-D} = 2\pi \int b \sum_{j_D} P_{ij_D}(b) db \quad (29)$$

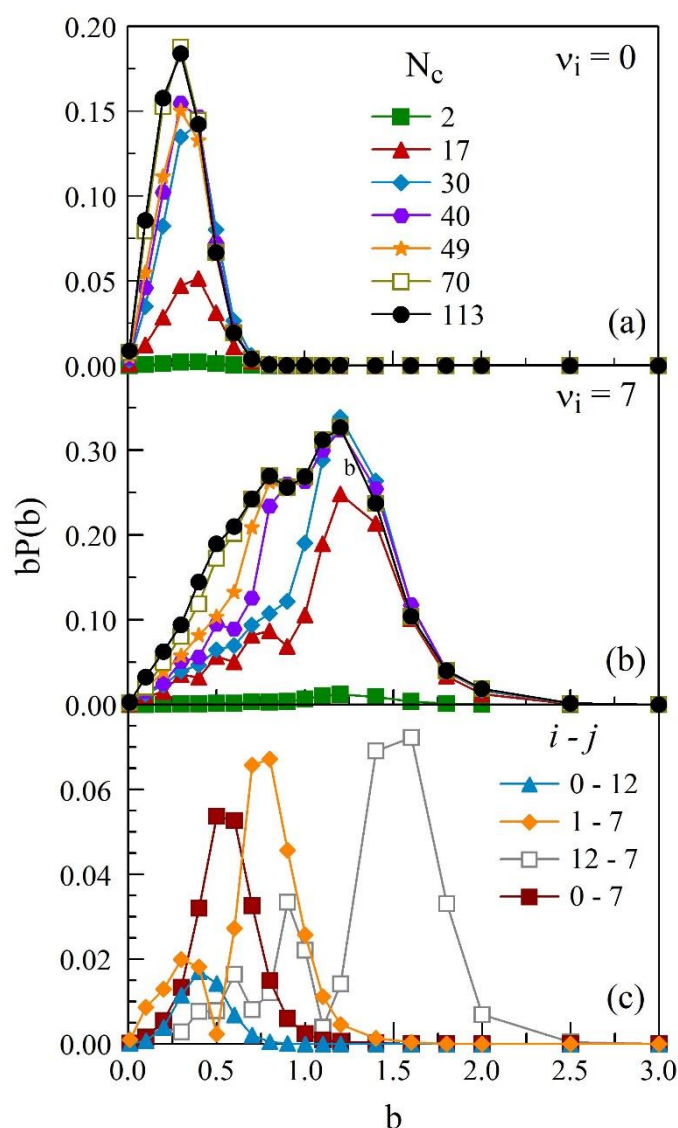


Fig. 7.  $bP(b)$  as functions of  $b$ , for dissociation of the vibrational states (a)  $i = 0$  and (b)  $i = 7$ , for various number of dissociative continuum states included. (c)  $bP(b)$  for typical bound-bound transitions, with  $N_c^{\max}$  continuum states (see text).

We found important to investigate how many states of the dissociative continuum is needed to be included in calculation of the  $S$  matrix terms to get reliable cross sections for the bound-bound transitions. We increased stepwise the number of continuum states from 2 to 113. The  $bP_{i-D}(b)$  for two typical cases of the initial state  $|i\rangle$ ,  $i = 0$  and  $i = 7$  are shown in Fig. 7a and 7b. Interestingly, the results with 70 and 113 continuum states vibrational states are almost identical, so we will consider that  $N_c^{\max} = 113$  continuum states are sufficient to obtain converged dissociation results. These 113 states span positive energy from 0 to  $\sim 5$  eV. In Fig. 7c we show  $bP(b)$  for a few typical bound-bound transitions, calculated with  $N_c^{\max}$  continuum states. We note that unitarity of the  $S$  matrix has been preserved in all calculations (to the 6 digits).

The cross sections for dissociation from various vibrational states, from the ground state ( $i = 0$ ) to the states close to the continuum edge ( $i = 12$ ) are shown in Fig. 8a, as functions of the number of included continuum states. The convergence of the results with 113 states, anticipated with the  $bP(b)$  curves, is here confirmed at the level of cross section within the predictably uncertainty. The uncertainty is documented in Fig. 8b, which shows relative deviation (in %) of the dissociation cross sections obtained with various number of included continua from the one computed with  $N_c^{\max} = 113$ . The deviations for  $N_c = 70$  are between a fraction of  $\sim 0.5\%$  and  $\sim 5\%$ .

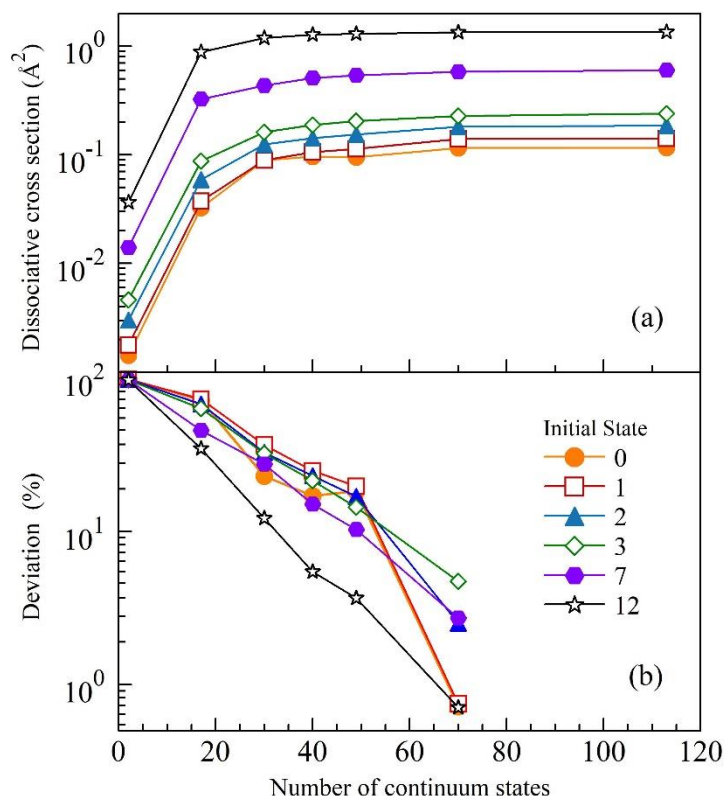


Fig. 8. (a) The cross section for dissociation versus the number of the included continuum states, form initial states  $v_i = 0, 1, 2, 7, 12$ . (b) The relative deviation between the cross sections of various total number of continuum states  $N_c$  and the cross section with  $N_c = 128$ .

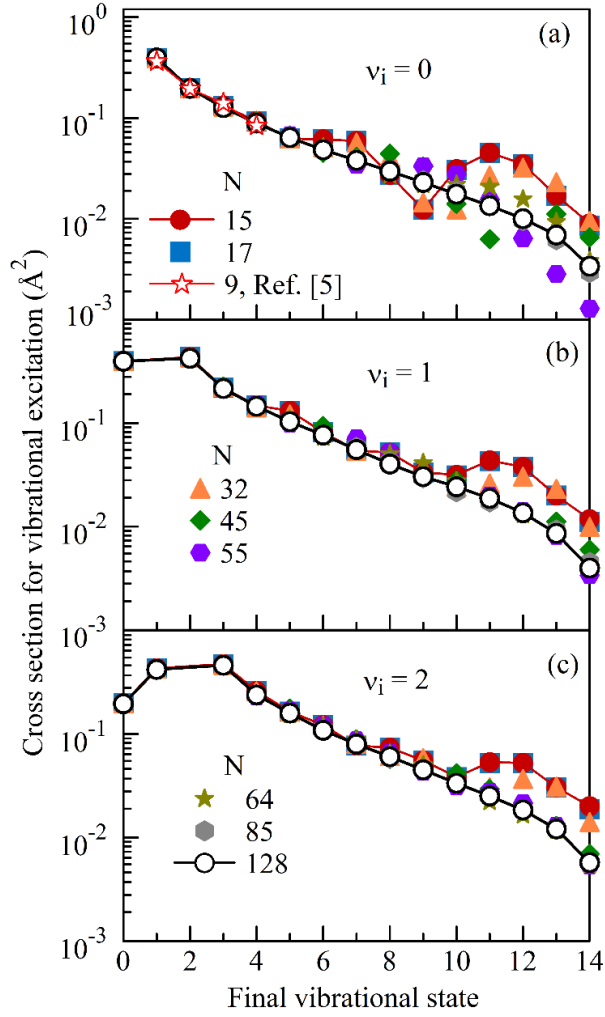


Fig. 9. The cross sections of inelastic transitions from (a) ground, (b) 1<sup>st</sup> excited and (c) 2<sup>nd</sup> excited vibrational state ( $v_i = 0, 1, 2$ ) to all other vibrational bound states in presence of dissociative continuum, for various total number of continuum states  $N_c$ .

The cross sections for transition from chosen initial to all bound vibrational states are shown in Figs. 9 and 10. Elastic cross sections are orders of magnitude above the inelastic cross sections shown here and are considered in this paper. Fig. 9a also contains comparison with a fully quantum calculations of the  $H + H_2$  collision system. The values of cross section in [9] were reported averaged over diatomic angle  $\gamma$ , and for some fixed angles. Since our calculation is done for  $\gamma = 90^\circ$ , we compare with the cross sections at that angle in [9]. The agreement is quite good although fully quantum calculation in [9] was one with only 9 bound vibrational states. This does not influence significantly the answer for excitations to the lower vibrational states, As seen in Fig. 9a, continuum states influence the transitions from the ground to the lower vibrational states only for final states larger than 5. Figs. 9b and 9c show that coupling to the continuum influences transitions from lower only to higher vibrational states.

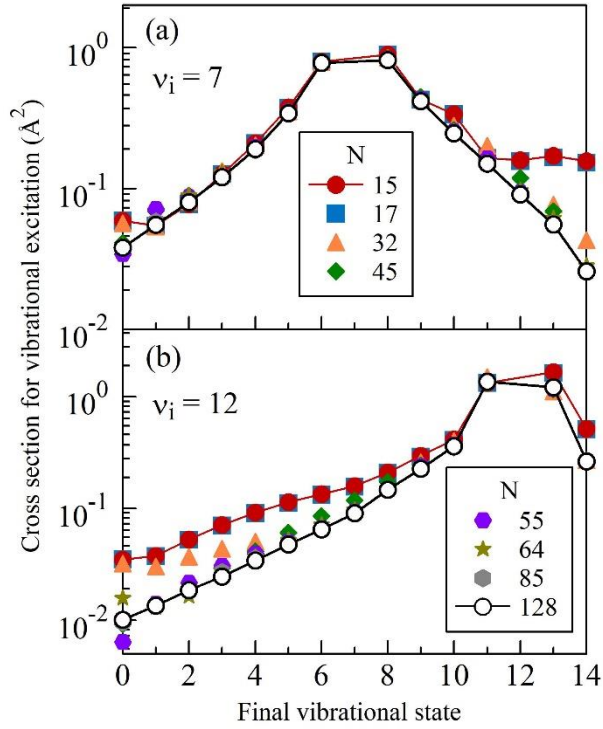


Fig. 10. The cross sections of inelastic transitions from (a) 7<sup>th</sup> excited and (b) 12<sup>th</sup> excited vibrational state ( $v_i = 7, 12$ ) to all other vibrational bounds states in presence of dissociative continuum, for various total number of continuum states  $N_c$ .

These conclusions have to be somewhat modified when initial state is a higher vibrational state, like are 7 and 12 in Fig. 10. For the initials state in the intermediate range ( $i = 7$ ), significant influence of the continuum appears in transition to the  $j \geq 10$ . However, if initial state is 12, transitions to both lower and higher states are persistently reduced by the presence of continuum, showing full convergence when  $N_c^{\max}$  continua is included in calculation.

Fig. 11 further quantify the uncertainty of the transitions among bound vibrational states of  $H_2$  in collision with  $H$  if dissociative continuum is included. Like in Fig. 8b, the relative deviations of the cross sections from chosen initial to all final bound states is included, when a various number of dissociation continua are taken into account where  $N_c^{\max}$  continua are shown. These are close to 5% for the case of  $N_c = 70$ , quantifying the upper bound of uncertainty of the bound-bound cross sections with  $N_c^{\max}$  continua are taken into account.

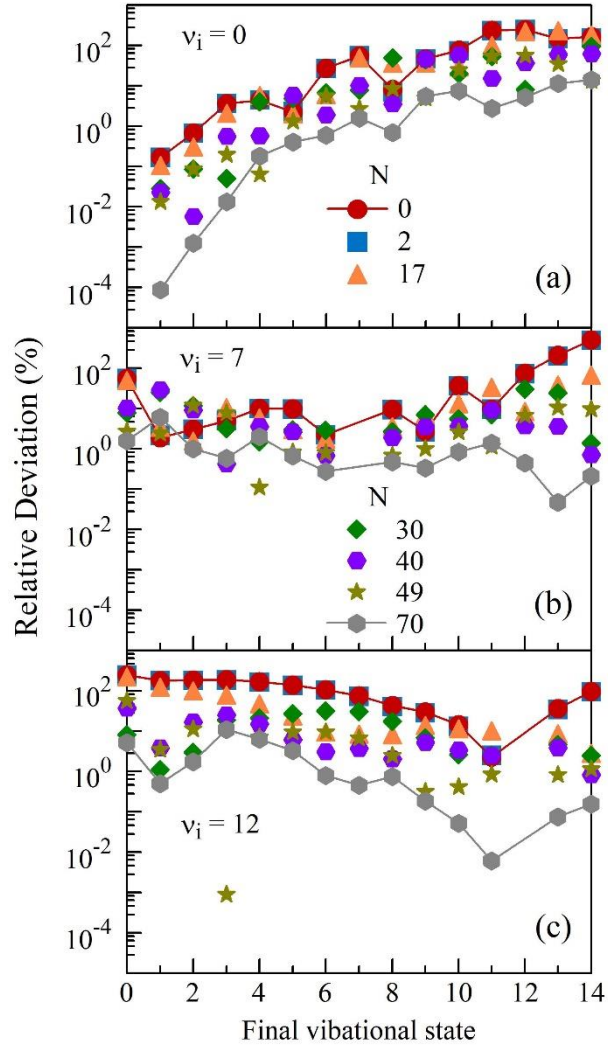


Fig. 11. The relative deviation between the cross sections with various number of continuum states  $N_c$  included and the converged cross sections of for  $N_c = 113$ , for vibrational excitation from the (a) ground, (b) 7<sup>th</sup> and (c) 12<sup>th</sup> vibrational states ( $v_i = 0, 7, 12$ ) to all other vibrational bound states.

On more factor of uncertainty deserves attention: Deviation of the results obtained using quantum circuit simulation and the benchmark results obtained by high accuracy ODE solver, as explained in Subsection 2.6. Fig. 12 shows maximal relative deviation (%) of these two families of the cross-section results, obtained using into account deviations of all states in a particular calculation. Interestingly main contributor to the deviation is the ground vibrational state, which contributes more than 5% to the uncertainty. All other states contribute to case of calculation with 128 states at about 1.5%.

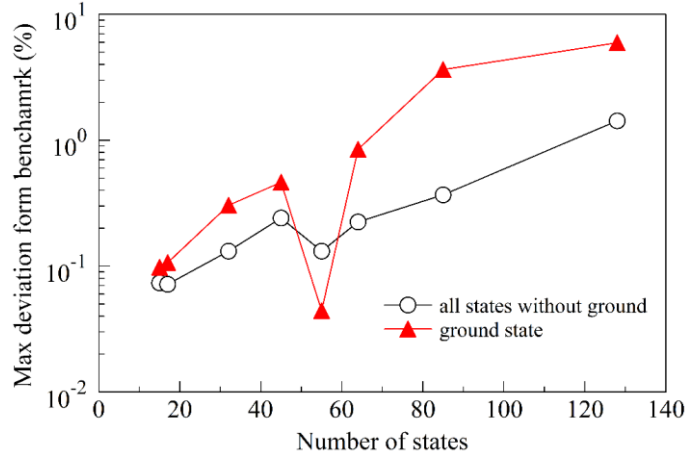


Fig. 12. Maximal relative deviation of the cross sections obtained quantum circuit simulations from the ODE benchmark results.

The method, shown in Section 2, can measure both phases and amplitudes of the  $S$  matrix. In case the initial state is a pure vibrational state, measurement can proceed with only  $|S_{ij}|^2$  i.e., with probabilities from a state  $|i\rangle$  to a state  $|j\rangle$ , which were used in calculations shown in this Section. Still, as an example we show in Sec. S2 of SM a full  $S$ -matrix, with both its real and imaginary parts, for bound-bound transitions, obtained for the  $H + H_2$  transitions in a set of 15 bound vibrational states. The simulation is carried out following the quantum algorithm shown in Fig. 6 and the results are obtained from gate-based simulator, PennyLane [15].

#### 4. CONCLUSIONS

The influence of the coupling of the vibrational states of  $H_2$  with the dissociative continuum to its transition vibrational dynamics was studied by colliding  $H_2$  with  $H$  at laboratory collision energy of 100 eV. The Born-Oppenheimer approximation is applied at the ground electronic surface of  $H_3$ . The quantum circuit is developed to compute the  $S$  matrix for transitions between bound and discretized dissociative continuum states, and the results were confirmed within a few percent's error using the comparison with the independent ODE approach for solution of time-dependent Schrodinger equation. With Inclusion of over hundred discrete continuum states, the convergence is reached with relative deviation of  $< 5\%$  of all bound-bound as well as total dissociation cross sections. Furthermore, the agreement is reached with available literature results at the used collision energy.

The cross sections for inelastic transitions between low laying vibrational states of  $H_2$  can be accurately calculated without inclusion of dissociative continua, at least at the considered collision energy. However, cross sections to or from higher vibrational states of  $H_2$ , require inclusion of dissociative continuum as deep as 5 eV of positive energy.

## REFERENCE

1. P. S. Krstic and D. R. Schultz, Elastic and vibrationally inelastic slow collisions:  $H+H_2$ ,  $H^++H_2$ , J. Phys. B: Ato. Mol. Opt. Phys 32, 2415 (1999).
2. P. S. Krstic and D. R. Schultz, Elastic processes involving vibrationally excited molecules in cold hydrogen plasma, J. Phys. B 36, 1 (2003).
3. R. K. Janev, D. Reiter and U. Samm, Collision processes in low-temperature hydrogen plasma, Berichte des Forschungszentrums Jülich; 4105, ISSN 0944-2952
4. M. Capitelli, R. Caliberto, O. De. Pascale, et al., Nuclear Fusion 46, S260 (2006)
5. P. S. Krstic and R. K. Janev, Inelastic processes from vibrationally excited states in slow  $H^++H_2$  and  $H+H_2^+$  collisions. Dissociation, Phys. Rev. A 67, 022708 (2003)
6. P. S. Krstic, Inelastic processes from vibrationally excited states in slow  $H^++H_2$  and  $H+H_2^+$ ; Excitations and charge transfer, Phys. Rev. A 66, 042717 (2002).
7. P. Benioff, The computer as a physical system: A microscopic quantum mechanical Hamiltonian model of computers as represented by Turing machines, J. Stat. Phys. **22**, 563 (1980).
8. R. P. Feynman, Simulating physics with computers, Int. J. Theor. Phys. **21**, 467 (1982).
9. P. S. Krstic and M. H. Mittleman, S-matrix theory of multiphoton ionization, J. Opt. Soc. Am. B 7, 587 (1990).
10. A. I. Boothroyd, A refined  $H_3$  potential energy surface, J. Chem Phys. 104, 7139 (1996).
11. Y. Shee, P.-K. Tsai, C.-L. Hong, H.-C. Cheng, and H.-S. Goan, A qubit-efficient encoding scheme for quantum simulations of electronic structure (2021), arXiv:2110.04112 [quant-ph].
12. A. Tranter, P. J. Love, F. Mintert, N. Wiebe and P. V. Coveney, Ordering of Trotterization: Impact on errors in quantum simulation of electronic structure, Entropy **21**, 1218 (2019).
13. M. A. Nielsen and I. L. Chuang, *Quantum Computation and Quantum Information: 10th Anniversary Edition*, 10th ed. (Cambridge University Press, USA, 2011).
14. P. Virtanen *et al.*, SciPy 1.0: Fundamental Algorithms for Scientific Computing in Python, Nat. Methods **17**, 261 (2020).
15. V. Bergholm *et al.*, PennyLane: Automatic differentiation of hybrid quantum-classical computations (2020), arXiv:1811.04968 [quant-ph].

## Supplemental Materials

### Collisional S-Matrix for the Vibrational Dynamics of H+H<sub>2</sub> Including Dissociative Processes by Quantum Computing

*Yulun Wang and Predrag S. Krstic*

Institute for Advanced Computational Science, Stony Brook University,  
Stony Brook NY 11794-5250

#### S1. QEE encoding of qubit Hamiltonian

Taking a general 4-state system, the qubit efficient encoding (QEE) for 2 qubits and 4 states gives:

$$\begin{aligned}
 H_q &= \sum_{i,j}^{N-1} h_{ij} |\mathbf{q}_i\rangle\langle\mathbf{q}_j| \\
 &= h_{00}|00\rangle\langle 00| + h_{11}|01\rangle\langle 01| + h_{22}|10\rangle\langle 10| + h_{33}|11\rangle\langle 11| \\
 &\quad + h_{01}|00\rangle\langle 01| + h_{10}|01\rangle\langle 00| + h_{12}|01\rangle\langle 10| + h_{21}|10\rangle\langle 01| \\
 &\quad + h_{13}|01\rangle\langle 11| + h_{31}|11\rangle\langle 01| + h_{02}|00\rangle\langle 10| + h_{20}|10\rangle\langle 00| \\
 &\quad + h_{03}|00\rangle\langle 11| + h_{30}|11\rangle\langle 00| + h_{23}|10\rangle\langle 11| + h_{32}|11\rangle\langle 10| \\
 &= h_{00}(|0\rangle\langle 0| \otimes |0\rangle\langle 0|) + h_{11}(|0\rangle\langle 0| \otimes |1\rangle\langle 1|) + h_{22}(|1\rangle\langle 1| \otimes |0\rangle\langle 0|) + h_{33}(|1\rangle\langle 1| \otimes |1\rangle\langle 1|) \\
 &\quad + h_{01}(|0\rangle\langle 0| \otimes |0\rangle\langle 1|) + h_{10}(|0\rangle\langle 0| \otimes |1\rangle\langle 0|) + h_{12}(|0\rangle\langle 1| \otimes |1\rangle\langle 0|) + h_{21}(|1\rangle\langle 0| \otimes |0\rangle\langle 1|) \\
 &\quad + h_{13}(|0\rangle\langle 1| \otimes |1\rangle\langle 1|) + h_{31}(|1\rangle\langle 0| \otimes |1\rangle\langle 1|) + h_{02}(|0\rangle\langle 1| \otimes |0\rangle\langle 0|) + h_{20}(|1\rangle\langle 0| \otimes |0\rangle\langle 0|) \\
 &\quad + h_{03}(|0\rangle\langle 1| \otimes |0\rangle\langle 1|) + h_{30}(|1\rangle\langle 0| \otimes |1\rangle\langle 0|) + h_{23}(|1\rangle\langle 1| \otimes |0\rangle\langle 1|) + h_{32}(|1\rangle\langle 1| \otimes |1\rangle\langle 0|) \\
 &= \frac{1}{4}(h_{00} + h_{11} + h_{22} + h_{33})I + \frac{1}{4}(h_{00} + h_{11} - h_{22} - h_{33})Z_0 + \frac{1}{4}(h_{00} - h_{11} + h_{22} - h_{33})Z_1 \\
 &\quad + \frac{1}{4}(h_{00} - h_{11} - h_{22} + h_{33})Z_0Z_1 + \frac{1}{4}(h_{13} + h_{31} + h_{02} + h_{20})X_0 + \frac{1}{4}(h_{01} + h_{10} + h_{23} + h_{32})X_1 \\
 &\quad + \frac{i}{4}(h_{13} - h_{31} + h_{02} - h_{20})Y_0 + \frac{i}{4}(h_{01} - h_{10} + h_{23} - h_{32})Y_1 - \frac{1}{4}(h_{13} + h_{31} + h_{02} + h_{20})X_0Z_1 \\
 &\quad - \frac{i}{4}(h_{13} - h_{31} - h_{02} + h_{20})Y_0Z_1 - \frac{1}{4}(h_{01} + h_{10} + h_{23} + h_{32})Z_0X_1 + \frac{i}{4}(h_{01} - h_{10} - h_{23} + h_{32})Z_0Y_1 \\
 &\quad + \frac{1}{4}(h_{12} + h_{21} + h_{03} + h_{30})X_0X_1 + \frac{1}{4}(h_{12} + h_{21} - h_{03} - h_{30})Y_0Y_1 - \frac{i}{4}(h_{12} - h_{21} - h_{03} + h_{30})X_0Y_1 \\
 &\quad + \frac{i}{4}(h_{12} - h_{21} + h_{03} - h_{30})Y_0X_1 \\
 &= g_0I + g_1Z_0 + g_2Z_1 + g_3Z_0Z_1 + g_4X_0 + g_5X_1 + g_6Y_0 + g_7Y_1 + g_8X_0Z_1 \\
 &\quad + g_9Y_0Z_1 + g_{10}Z_0X_1 + g_{11}Z_0Y_1 + g_{12}X_0X_1 + g_{13}Y_0Y_1 + g_{14}X_0Y_1 + g_{15}Y_0X_1 \tag{S1}
 \end{aligned}$$

where

$$\begin{aligned}
g_0 &= \frac{1}{4}(h_{00} + h_{11} + h_{22} + h_{33}), g_1 = \frac{1}{4}(h_{00} + h_{11} - h_{22} - h_{33}) \\
g_2 &= \frac{1}{4}(h_{00} - h_{11} + h_{22} - h_{33}), g_3 = \frac{1}{4}(h_{00} - h_{11} - h_{22} + h_{33}) \\
g_4 &= \frac{1}{4}(h_{13} + h_{31} + h_{02} + h_{20}), g_5 = \frac{1}{4}(h_{01} + h_{10} + h_{23} + h_{32}) \\
g_6 &= \frac{i}{4}(h_{13} - h_{31} + h_{02} - h_{20}), g_7 = \frac{i}{4}(h_{01} - h_{10} + h_{23} - h_{32}) \\
g_8 &= -\frac{1}{4}(h_{13} + h_{31} + h_{02} + h_{20}), g_9 = -\frac{i}{4}(h_{13} - h_{31} - h_{02} + h_{20}) \\
g_{10} &= -\frac{1}{4}(h_{01} + h_{10} + h_{23} + h_{32}), g_{11} = \frac{i}{4}(h_{01} - h_{10} - h_{23} + h_{32}) \\
g_{12} &= +\frac{1}{4}(h_{12} + h_{21} + h_{03} + h_{30}), g_{13} = \frac{1}{4}(h_{12} + h_{21} - h_{03} - h_{30}) \\
g_{14} &= -\frac{i}{4}(h_{12} - h_{21} - h_{03} + h_{30}), g_{15} = \frac{i}{4}(h_{12} - h_{21} + h_{03} - h_{30})
\end{aligned} \tag{S2}$$

## S2. S-matrix calculation by quantum algorithm

In this section, we show a full  $S$ -matrix, with both its real and imaginary parts, for bound-bound transitions, obtained for the  $H + H_2$  transitions in a set of 15 bound vibrational states. The simulation is carried out following the quantum algorithm shown in Fig. 6 and the results are obtained from gate-based simulator, PennyLane [15].

Table S1. The  $S$  matrix elements for transitions from initial state  $i = 0,1,2$  to final state  $j = 0,1, \dots, 14$ , obtained by quantum simulation.

| $i = 0$   |              |              | $i = 1$   |              |              | $i = 2$   |              |              |
|-----------|--------------|--------------|-----------|--------------|--------------|-----------|--------------|--------------|
| $j$       | $Re[S_{ij}]$ | $Im[S_{ij}]$ | $j$       | $Re[S_{ij}]$ | $Im[S_{ij}]$ | $j$       | $Re[S_{ij}]$ | $Im[S_{ij}]$ |
| <b>0</b>  | -3.199e-02   | -1.005e-01   | <b>0</b>  | 1.139e-01    | -1.729e-01   | <b>0</b>  | -2.632e-01   | -2.628e-02   |
| <b>1</b>  | 1.142e-01    | -1.727e-01   | <b>1</b>  | 3.250e-01    | -4.635e-02   | <b>1</b>  | -1.595e-01   | -3.158e-01   |
| <b>2</b>  | -2.631e-01   | -2.725e-02   | <b>2</b>  | -1.590e-01   | -3.161e-01   | <b>2</b>  | -1.424e-01   | 3.671e-01    |
| <b>3</b>  | 4.297e-03    | -2.808e-01   | <b>3</b>  | 2.549e-01    | -2.874e-01   | <b>3</b>  | -6.341e-03   | 1.574e-01    |
| <b>4</b>  | -3.332e-01   | -3.642e-03   | <b>4</b>  | -1.318e-01   | -2.214e-02   | <b>4</b>  | -1.826e-01   | -1.287e-01   |
| <b>5</b>  | -1.917e-02   | 2.673e-01    | <b>5</b>  | -1.609e-01   | -1.555e-01   | <b>5</b>  | 1.059e-01    | -1.116e-01   |
| <b>6</b>  | 1.345e-01    | 1.948e-01    | <b>6</b>  | -9.925e-03   | 2.647e-01    | <b>6</b>  | -3.887e-01   | 2.332e-01    |
| <b>7</b>  | -3.636e-01   | 5.811e-02    | <b>7</b>  | 9.746e-03    | 1.638e-01    | <b>7</b>  | -2.664e-01   | -1.010e-01   |
| <b>8</b>  | -2.574e-02   | 3.237e-01    | <b>8</b>  | 1.187e-01    | -2.360e-01   | <b>8</b>  | 1.366e-01    | -1.019e-01   |
| <b>9</b>  | -8.424e-02   | -1.051e-01   | <b>9</b>  | 1.833e-01    | 8.549e-04    | <b>9</b>  | 2.828e-01    | 2.171e-01    |
| <b>10</b> | -3.778e-02   | -1.871e-01   | <b>10</b> | -1.492e-01   | -3.662e-02   | <b>10</b> | 2.000e-01    | -1.428e-01   |
| <b>11</b> | 2.399e-01    | 1.910e-01    | <b>11</b> | 6.066e-02    | -2.862e-01   | <b>11</b> | -3.038e-02   | 4.182e-02    |
| <b>12</b> | -3.007e-01   | -6.314e-03   | <b>12</b> | 2.012e-01    | 2.419e-01    | <b>12</b> | 1.014e-01    | 1.556e-02    |
| <b>13</b> | -2.076e-01   | 7.455e-02    | <b>13</b> | 2.252e-01    | 9.538e-02    | <b>13</b> | 1.200e-01    | -1.246e-02   |
| <b>14</b> | 1.540e-01    | -7.629e-02   | <b>14</b> | -1.987e-01   | -2.693e-02   | <b>14</b> | -1.344e-01   | 4.960e-02    |

Table S2. The S matrix elements for transitions from initial state  $i = 3,4,5$  to final state  $j = 0,1, \dots,14$ , obtained by quantum simulation.

| $i = 3$   |              |              | $i = 4$   |              |              | $i = 5$   |              |              |
|-----------|--------------|--------------|-----------|--------------|--------------|-----------|--------------|--------------|
| $j$       | $Re[S_{ij}]$ | $Im[S_{ij}]$ | $j$       | $Re[S_{ij}]$ | $Im[S_{ij}]$ | $j$       | $Re[S_{ij}]$ | $Im[S_{ij}]$ |
| <b>0</b>  | 2.789e-03    | -2.809e-01   | <b>0</b>  | -3.332e-01   | -1.326e-03   | <b>0</b>  | -1.692e-02   | 2.674e-01    |
| <b>1</b>  | 2.539e-01    | -2.882e-01   | <b>1</b>  | -1.319e-01   | -2.148e-02   | <b>1</b>  | -1.619e-01   | -1.545e-01   |
| <b>2</b>  | -6.076e-03   | 1.574e-01    | <b>2</b>  | -1.830e-01   | -1.282e-01   | <b>2</b>  | 1.054e-01    | -1.121e-01   |
| <b>3</b>  | 1.779e-01    | 1.138e-01    | <b>3</b>  | 1.200e-01    | 2.886e-01    | <b>3</b>  | 3.129e-02    | -5.670e-01   |
| <b>4</b>  | 1.195e-01    | 2.888e-01    | <b>4</b>  | -1.593e-01   | -5.603e-01   | <b>4</b>  | 8.773e-02    | 7.962e-02    |
| <b>5</b>  | 3.303e-02    | -5.669e-01   | <b>5</b>  | 8.762e-02    | 7.975e-02    | <b>5</b>  | 1.399e-01    | 1.756e-02    |
| <b>6</b>  | -4.433e-02   | 1.508e-01    | <b>6</b>  | 7.600e-03    | 4.558e-02    | <b>6</b>  | -4.896e-01   | -1.516e-01   |
| <b>7</b>  | 1.398e-01    | 1.493e-01    | <b>7</b>  | 2.065e-01    | 2.937e-01    | <b>7</b>  | -5.959e-02   | -2.491e-02   |
| <b>8</b>  | 6.283e-03    | -2.801e-02   | <b>8</b>  | 5.510e-02    | -2.111e-01   | <b>8</b>  | 1.386e-01    | -2.118e-01   |
| <b>9</b>  | -1.643e-01   | -4.441e-02   | <b>9</b>  | -1.135e-01   | -1.670e-01   | <b>9</b>  | 3.258e-02    | -9.773e-02   |
| <b>10</b> | -1.269e-03   | 1.167e-01    | <b>10</b> | -2.165e-01   | 1.666e-01    | <b>10</b> | -1.792e-01   | 1.181e-01    |
| <b>11</b> | -3.765e-02   | 1.351e-01    | <b>11</b> | -1.851e-02   | -8.388e-02   | <b>11</b> | -5.986e-02   | -5.851e-02   |
| <b>12</b> | -1.790e-01   | -1.510e-01   | <b>12</b> | -8.107e-02   | -3.609e-02   | <b>12</b> | -6.479e-02   | -1.059e-01   |
| <b>13</b> | -2.196e-01   | -4.277e-02   | <b>13</b> | -1.494e-01   | -5.806e-03   | <b>13</b> | -1.801e-01   | -6.441e-02   |
| <b>14</b> | 2.163e-01    | -5.176e-02   | <b>14</b> | 1.732e-01    | -9.243e-02   | <b>14</b> | 2.120e-01    | -8.092e-02   |

Table S3. The S matrix elements for transitions from initial state  $i = 6,7,8$  to final state  $j = 0,1, \dots,14$ , obtained by quantum simulation.

| $i = 6$   |              |              | $i = 7$   |              |              | $i = 8$   |              |              |
|-----------|--------------|--------------|-----------|--------------|--------------|-----------|--------------|--------------|
| $j$       | $Re[S_{ij}]$ | $Im[S_{ij}]$ | $j$       | $Re[S_{ij}]$ | $Im[S_{ij}]$ | $j$       | $Re[S_{ij}]$ | $Im[S_{ij}]$ |
| <b>0</b>  | 1.364e-01    | 1.934e-01    | <b>0</b>  | -3.630e-01   | 6.213e-02    | <b>0</b>  | -2.178e-02   | 3.240e-01    |
| <b>1</b>  | -7.833e-03   | 2.648e-01    | <b>1</b>  | 1.125e-02    | 1.637e-01    | <b>1</b>  | 1.163e-01    | -2.372e-01   |
| <b>2</b>  | -3.872e-01   | 2.356e-01    | <b>2</b>  | -2.671e-01   | -9.899e-02   | <b>2</b>  | 1.357e-01    | -1.031e-01   |
| <b>3</b>  | -4.366e-02   | 1.510e-01    | <b>3</b>  | 1.406e-01    | 1.485e-01    | <b>3</b>  | 6.091e-03    | -2.805e-02   |
| <b>4</b>  | 7.730e-03    | 4.556e-02    | <b>4</b>  | 2.077e-01    | 2.928e-01    | <b>4</b>  | 5.398e-02    | -2.114e-01   |
| <b>5</b>  | -4.898e-01   | -1.509e-01   | <b>5</b>  | -5.966e-02   | -2.475e-02   | <b>5</b>  | 1.378e-01    | -2.123e-01   |
| <b>6</b>  | -1.409e-02   | -3.129e-02   | <b>6</b>  | -2.091e-01   | -1.798e-01   | <b>6</b>  | 3.014e-01    | 6.866e-02    |
| <b>7</b>  | -2.089e-01   | -1.801e-01   | <b>7</b>  | -3.194e-01   | 7.004e-02    | <b>7</b>  | -2.550e-01   | -1.170e-01   |
| <b>8</b>  | 3.012e-01    | 6.939e-02    | <b>8</b>  | -2.549e-01   | -1.173e-01   | <b>8</b>  | 3.084e-01    | 2.475e-01    |
| <b>9</b>  | 2.925e-02    | 1.614e-02    | <b>9</b>  | -1.241e-01   | -3.961e-01   | <b>9</b>  | 3.189e-03    | -2.184e-01   |
| <b>10</b> | -2.688e-01   | 1.062e-01    | <b>10</b> | 2.371e-02    | 5.973e-02    | <b>10</b> | -5.059e-03   | 3.494e-01    |
| <b>11</b> | -4.963e-02   | -2.098e-01   | <b>11</b> | 4.170e-02    | 1.117e-01    | <b>11</b> | -2.737e-01   | 1.004e-01    |
| <b>12</b> | 3.847e-02    | -5.121e-02   | <b>12</b> | -6.698e-02   | 1.180e-01    | <b>12</b> | -9.084e-03   | -5.146e-02   |
| <b>13</b> | -1.231e-01   | -9.098e-02   | <b>13</b> | 1.196e-01    | 1.893e-01    | <b>13</b> | 7.443e-02    | 1.520e-01    |
| <b>14</b> | 1.998e-01    | -8.642e-02   | <b>14</b> | -2.435e-01   | 3.607e-02    | <b>14</b> | -2.530e-01   | 4.975e-02    |

Table S4. The S matrix elements for transitions from initial state  $i = 9,10,11$  to final state  $j = 0,1, \dots, 14$ , obtained by quantum simulation.

| $i = 9$   |              |              | $i = 10$  |              |              | $i = 11$  |              |              |
|-----------|--------------|--------------|-----------|--------------|--------------|-----------|--------------|--------------|
| $j$       | $Re[S_{ij}]$ | $Im[S_{ij}]$ | $j$       | $Re[S_{ij}]$ | $Im[S_{ij}]$ | $j$       | $Re[S_{ij}]$ | $Im[S_{ij}]$ |
| <b>0</b>  | -8.563e-02   | -1.040e-01   | <b>0</b>  | -4.043e-02   | -1.866e-01   | <b>0</b>  | 2.427e-01    | 1.874e-01    |
| <b>1</b>  | 1.833e-01    | -1.230e-03   | <b>1</b>  | -1.497e-01   | -3.478e-02   | <b>1</b>  | 5.691e-02    | -2.869e-01   |
| <b>2</b>  | 2.848e-01    | 2.144e-01    | <b>2</b>  | 1.985e-01    | -1.449e-01   | <b>2</b>  | -2.990e-02   | 4.216e-02    |
| <b>3</b>  | -1.646e-01   | -4.312e-02   | <b>3</b>  | -2.391e-04   | 1.167e-01    | <b>3</b>  | -3.635e-02   | 1.355e-01    |
| <b>4</b>  | -1.146e-01   | -1.663e-01   | <b>4</b>  | -2.153e-01   | 1.682e-01    | <b>4</b>  | -1.919e-02   | -8.373e-02   |
| <b>5</b>  | 3.211e-02    | -9.789e-02   | <b>5</b>  | -1.785e-01   | 1.191e-01    | <b>5</b>  | -6.024e-02   | -5.811e-02   |
| <b>6</b>  | 2.930e-02    | 1.604e-02    | <b>6</b>  | -2.684e-01   | 1.074e-01    | <b>6</b>  | -5.072e-02   | -2.095e-01   |
| <b>7</b>  | -1.250e-01   | -3.958e-01   | <b>7</b>  | 2.389e-02    | 5.965e-02    | <b>7</b>  | 4.214e-02    | 1.115e-01    |
| <b>8</b>  | 2.961e-03    | -2.184e-01   | <b>8</b>  | -4.371e-03   | 3.495e-01    | <b>8</b>  | -2.734e-01   | 1.011e-01    |
| <b>9</b>  | -3.233e-01   | -3.718e-01   | <b>9</b>  | 6.286e-02    | 1.553e-02    | <b>9</b>  | 3.286e-01    | -1.807e-01   |
| <b>10</b> | 6.285e-02    | 1.559e-02    | <b>10</b> | -1.344e-01   | 5.638e-01    | <b>10</b> | 1.188e-01    | 1.651e-01    |
| <b>11</b> | 3.289e-01    | -1.802e-01   | <b>11</b> | 1.187e-01    | 1.652e-01    | <b>11</b> | 5.130e-01    | -2.120e-01   |
| <b>12</b> | 1.147e-01    | 2.298e-01    | <b>12</b> | 1.110e-01    | 1.887e-01    | <b>12</b> | 1.527e-01    | -2.267e-01   |
| <b>13</b> | 1.113e-01    | -1.446e-01   | <b>13</b> | 2.313e-01    | -1.687e-01   | <b>13</b> | -1.905e-01   | 8.262e-02    |
| <b>14</b> | 1.812e-01    | -9.086e-03   | <b>14</b> | 1.365e-01    | 7.377e-02    | <b>14</b> | -1.383e-01   | -1.049e-01   |

Table S5. The S matrix elements for transitions from initial state  $i = 12,13,14$  to final state  $j = 0,1, \dots, 14$ , obtained by quantum simulation.

| $i = 12$  |              |              | $i = 13$  |              |              | $i = 14$  |              |              |
|-----------|--------------|--------------|-----------|--------------|--------------|-----------|--------------|--------------|
| $j$       | $Re[S_{ij}]$ | $Im[S_{ij}]$ | $j$       | $Re[S_{ij}]$ | $Im[S_{ij}]$ | $j$       | $Re[S_{ij}]$ | $Im[S_{ij}]$ |
| <b>0</b>  | -3.008e-01   | -1.613e-03   | <b>0</b>  | -2.064e-01   | 7.788e-02    | <b>0</b>  | 1.527e-01    | -7.880e-02   |
| <b>1</b>  | 2.045e-01    | 2.391e-01    | <b>1</b>  | 2.265e-01    | 9.217e-02    | <b>1</b>  | -1.991e-01   | -2.404e-02   |
| <b>2</b>  | 1.016e-01    | 1.434e-02    | <b>2</b>  | 1.199e-01    | -1.395e-02   | <b>2</b>  | -1.337e-01   | 5.130e-02    |
| <b>3</b>  | -1.806e-01   | -1.492e-01   | <b>3</b>  | -2.200e-01   | -4.041e-02   | <b>3</b>  | 2.157e-01    | -5.414e-02   |
| <b>4</b>  | -8.138e-02   | -3.539e-02   | <b>4</b>  | -1.494e-01   | -4.437e-03   | <b>4</b>  | 1.723e-01    | -9.406e-02   |
| <b>5</b>  | -6.555e-02   | -1.054e-01   | <b>5</b>  | -1.806e-01   | -6.302e-02   | <b>5</b>  | 2.114e-01    | -8.261e-02   |
| <b>6</b>  | 3.817e-02    | -5.144e-02   | <b>6</b>  | -1.237e-01   | -9.020e-02   | <b>6</b>  | 1.993e-01    | -8.774e-02   |
| <b>7</b>  | -6.644e-02   | 1.183e-01    | <b>7</b>  | 1.205e-01    | 1.886e-01    | <b>7</b>  | -2.433e-01   | 3.736e-02    |
| <b>8</b>  | -9.259e-03   | -5.143e-02   | <b>8</b>  | 7.502e-02    | 1.517e-01    | <b>8</b>  | -2.527e-01   | 5.080e-02    |
| <b>9</b>  | 1.152e-01    | 2.295e-01    | <b>9</b>  | 1.109e-01    | -1.449e-01   | <b>9</b>  | 1.812e-01    | -9.652e-03   |
| <b>10</b> | 1.112e-01    | 1.886e-01    | <b>10</b> | 2.310e-01    | -1.691e-01   | <b>10</b> | 1.366e-01    | 7.347e-02    |
| <b>11</b> | 1.525e-01    | -2.268e-01   | <b>11</b> | -1.904e-01   | 8.284e-02    | <b>11</b> | -1.385e-01   | -1.047e-01   |
| <b>12</b> | -4.509e-01   | -4.222e-01   | <b>12</b> | 3.428e-01    | -3.140e-03   | <b>12</b> | 2.719e-02    | 9.022e-02    |
| <b>13</b> | 3.428e-01    | -2.976e-03   | <b>13</b> | -2.681e-02   | 4.823e-01    | <b>13</b> | 3.942e-01    | 3.422e-02    |
| <b>14</b> | 2.712e-02    | 9.024e-02    | <b>14</b> | 3.942e-01    | 3.433e-02    | <b>14</b> | 4.903e-01    | -3.207e-01   |